Acta Crystallographica Section D
Biological Crystallography
ISSN 0907-4449

Crystallographic phasing of myristoyl-CoA–protein *N*-myristoyltransferase using an iodinated analog of myristoyl-CoA

Klaus Fütterer,[a]†‡ Clare L. Murray,[b]† Rajiv S. Bhatnagar,[b]† George W. Gokel,[b,c] Jeffrey I. Gordon[b] and Gabriel Waksman[a]*

[a]Department of Biochemistry and Molecular Biophysics, Washington University School of Medicine, Campus Box 8231, 660 S. Euclid Avenue, Saint Louis, MO 63110, USA, [b]Department of Molecular Biology and Pharmacology, Washington University School of Medicine, Campus Box 8231, 660 S. Euclid Avenue, Saint Louis, MO 63110, USA, and [c]Bioorganic Chemistry Program, Washington University School of Medicine, Campus Box 8231, 660 S. Euclid Avenue, Saint Louis, MO 63110, USA

† These authors contributed equally to this work.
‡ Present address: School of Biosciences, University of Birmingham, Edgbaston, Birmingham B15 2TT, England.

Correspondence e-mail: waksman@biochem.wustl.edu

Received 22 August 2000
Accepted 4 January 2001

Myristoyl-CoA–protein *N*-myristoyltransferase (Nmt; E.C. 2.1.3.97) catalyzes the covalent attachment of myristate to the N-terminal glycine amine of many eukaryotic and viral proteins. The molecular structure of the ternary complex of *Saccharomyces cerevisiae* Nmt1p with a bound non-hydrolyzable myristoyl-CoA analog, *S*-(2-oxopentadecyl)-CoA, and a competitive peptidomimetic inhibitor, SC-58272, was solved to 2.9 Å resolution by X-ray crystallography. The structure determination utilized diffraction data from an iodinated ternary complex in which a newly designed and synthesized compound, *S*-(13-iodo-2-oxotridecyl)-CoA, was substituted for *S*-(2-oxopentadecyl)-CoA. Replacing the two terminal fatty acid C atoms of myristate by iodine produced, under the same crystallization conditions, heavy-atom-derivatized crystals of defined site occupancy that were isomorphous to the native complex. This approach for obtaining experimental phase information can be extended to other crystal structures of protein–fatty acyl complexes. The synthesis of *S*-(13-iodo-2-oxotridecyl)-CoA and the phasing procedure are described.

1. Introduction

Myristoyl-CoA–protein *N*-myristoyltransferase (Nmt; E.C. 2.1.3.97) catalyzes the co-translational covalent attachment of the 14-carbon saturated fatty acid myristate ($C_{14:0}$) to the N-terminal glycine of a subset of cellular and viral proteins. The attachment, by an amide bond, requires a glycine residue at the N-terminus and is generally considered to be irreversible (Bhatnagar & Gordon, 1997). In general, myristate functions to promote relatively weak interactions of *N*-myristoyl proteins with membrane lipids or other proteins. Thus, these interactions can be severed with modest thermodynamic cost (Bhatnagar *et al.*, 2000).

The enzymatic reaction catalyzed by Nmt follows a Bi Bi ordered reaction mechanism: myristoyl coenzyme A, the lipid donor, binds first followed by the nascent peptide substrate; following catalysis, CoA and then the myristoylpeptide are released (Rudnick *et al.*, 1991). Recently, we determined the structure of *S. cerevisiae* Nmt (Nmt1p) in a ternary complex with a non-hydrolyzable myristoyl-CoA analog and dipeptide inhibitor (Bhatnagar *et al.*, 1998). The structure of this monomeric enzyme provided a structure-based model for its catalytic and kinetic reaction mechanisms (Bhatnagar *et al.*, 1998, 1999). The substrate analogs contained in this complex were *S*-(2-oxopentadecyl)-CoA (Paige *et al.*, 1989), substituting for myristoyl-CoA, and a peptidomimetic inhibitor, SC-58272 (Devadas *et al.*, 1995). *S*-(2-oxopentadecyl)-CoA differs from the natural ligand by an additional methylene group (C′ in Fig. 1*a*) interposed between the sulfur of pante-

theine and the carbonyl carbon of myristate. The competitive dipeptide inhibitor SC-5827 is derived from an octapeptide substrate, GLYASKLS, representing the N-terminal sequence of a known yeast *N*-myristoyl protein (Devadas *et al.*, 1995; Bhatnagar *et al.*, 1997). Only Ser and Lys, critical determinants of binding specificity and affinity, are retained in the peptidomimetic inhibitor (Fig. 1*c*).

Phase information from three-wavelength anomalous diffraction data of a selenomethionine (SeMet)-substituted Nmt1p with bound *S*-(2-oxopentadecyl)-CoA and SC-58272 was insufficient to construct a complete model of the Nmt1p ternary complex. Numerous attempts at soaking Nmt1p ternary complex crystals in heavy-metal salt solutions failed to produce a heavy-atom derivative, prompting us to consider chemical modification of one of the substrate analogs. Here, we describe the synthesis of a novel iodine-containing non-hydrolyzable coenzyme A derivative (I), *S*-(13-iodo-2-oxotridecyl)-CoA (Fig. 1*b*), wherein a single I atom replaces the ω-terminal C atoms 13 and 14 of the myristate moiety of *S*-(2-oxopentadecyl)-CoA. Crystals of Nmt1p with bound *S*-(13-iodo-2-oxotridecyl)-CoA and SC-58272 were obtained under the same conditions as the original ternary complex and provided diffraction data of similar quality. An improved experimental electron-density map was obtained when these iodo-derivative data (one iodine site) together with the SeMet MAD data (four selenium sites) were used in phasing. These results suggest that chemical modification of fatty acid ligands may be a generally useful route to obtain heavy-atom derivatives of protein–lipid complexes.

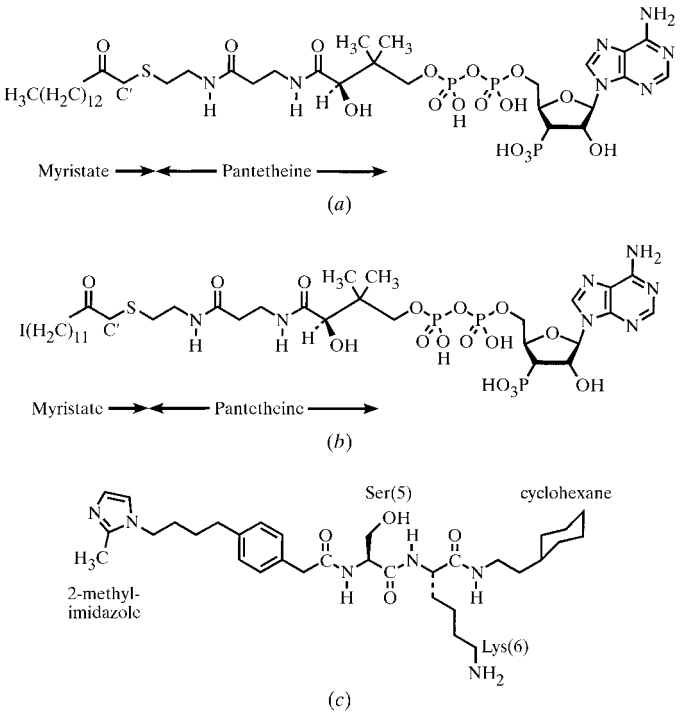

Figure 1
Chemical structure of the substrate analogs of *S. cerevisiae* Nmt1p. (*a*) *S*-(2-oxopentadecyl)-CoA. (*b*) The iodinated non-hydrolyzable myristoyl-CoA analog *S*-(13-iodo-2-oxotridecyl)-CoA. (*c*) The dipeptide substrate analog SC-58272.

2. Procedures

2.1. Protein expression and purification

Purification of Nmt1p and crystallization of the ternary Nmt1p–*S*-(2-oxopentadecyl)-CoA–SC-58272 complex has been described (Bhatnagar *et al.*, 1998). The ternary complex of Nmt1p with *S*-(13-iodo-2-oxotridecyl)-CoA and SC-58272 was obtained in a similar fashion.

2.2. Design of the iodinated non-hydrolyzable myristoyl-CoA analog

Four primary issues were considered in the design of the myristoyl-CoA analog. Firstly, it would have to incorporate an atom of sufficient size and scattering power to make it useful for crystal structure determination. Secondly, the derivative would have to be sufficiently similar in structure to known ligands so that it could be interchanged with one of them. Thirdly, the derivative would have to be chemically stable and not reactive with the protein backbone or any amino-acid side chains. Fourthly and finally, the chosen target compound would have to be synthetically accessible.

The non-hydrolyzable coenzyme A derivative *S*-(2-oxopentadecyl)-CoA is sterically equivalent to pentadecanoyl CoA. The two compounds may be represented as $CH_3(CH_2)_{12}COCH_2-S-CoA$ and $CH_3(CH_2)_{13}CO-S-CoA$. The myristoyl ($C_{14:0}$) unit of the former is separated by a methylene from coenzyme A, to which it is attached by a thioether link. The addition of the methylene unit between the carbonyl and sulfur makes the system non-hydrolyzable but also extends the length by $\sim$1 Å overall. In designing a heavy-atom derivative, we sought to maintain the size of the non-hydrolyzable derivative by replacing the appropriate number of methylene groups by the heavy atom.

Initial consideration focused on the use of divalent atoms such as zinc (Z = 30), cadmium (Z = 48), mercury (Z = 80), selenium (Z = 34) and tellurium (Z = 52). Mercury, being the heaviest, was considered to be the prime candidate for use in a synthetic ligand. However, group IIB elements Zn, Cd and Hg (*i.e.* those having $4s^2$, $5s^2$ and $6s^2$ electronic configurations) are reactive organometallic reagents. Incorporation of any of these metals could lead to a reactive ligand that might chemically modify the enzyme rather than simply occupy its binding site. A survey of the literature revealed that similar hazards attended the use of Se and Te.

Bromine and iodine are both attractive as heavy-metal substitution derivatives since they can be incorporated by a variety of synthetic methods. In previous work, we demonstrated that F, Cl and Br could all be accommodated within the binding pocket when they were present in synthetic fatty acid derivatives (Lu *et al.*, 1994). Indeed, 13-bromotridecanoyl-CoA [$Br(CH_2)_{12}CO-S-CoA$] was found to have an activity indistinguishable from that of myristoyl-CoA in a single point assay (Kishore *et al.*, 1991).

An important feature of halogens is that they are typically monovalent and therefore must be a terminal substituent in an unbranched fatty acid. Moreover, the halogens differ in size: F < Cl $\simeq$ Br < I. Iodide is generally considered to be a better

leaving group than bromide, but concern about stability was offset by iodine's greater atomic number. The higher atomic number obviously portended greater visibility in an X-ray electron-density map. However, it also meant that a chain-length adjustment might be required. The van der Waals radius of iodine is 2.15 Å, making it somewhat larger than a methyl group (2.0 Å) but smaller than ethyl. Thus, replacement of either one or two C atoms was possible. For synthetic reasons relating to starting material availability, we elected to replace the ultimate and penultimate C atoms of $CH_3(CH_2)_{12}COCH_2-S-CoA$ with a single terminal iodine to give (I).

The target compound (I) is the iodinated non-hydrolyzable CoA derivative shown in Fig. 1(*b*). It is based in part on the non-halogenated non-hydrolyzable CoA derivative reported by Paige *et al.* (1989). The strategy was to prepare $I(CH_2)_{11}COCH_2I$ and then alkylate CoASH. Although two primary iodides are present in this precursor, only one is activated by a geminal carbonyl group. Alkylation should therefore proceed readily to form (I).

Synthesis of (I) was accomplished according to Fig. 2. Baeyer–Villiger oxidation of commercial cyclododecanone gave 2-oxacyclotridecanone. Hydrolysis of the lactone afforded the ω-hydroxyacid. Conversion of the hydroxyacid into the corresponding bromoacid [$Br(CH_2)_{11}COOH$] was accomplished by treatment with HBr in acetic acid. The bromoacid was converted into the acid chloride [$Br(CH_2)_{11}COCl$] by treatment with thionyl chloride ($SOCl_2$). Reaction of the acid chloride with diazomethane (CH_2N_2) gave the diazoketone [$Br(CH_2)_{11}COCHN_2$], which was converted into the dibromide by treatment with HBr. Both Br atoms were then exchanged by using the Finkelstein procedure (NaI, acetone) to produce $I(CH_2)_{11}COCH_2I$.

The coenzyme A derivative was prepared by adding an ethanolic solution of 1,13-diiodotridecan-2-one to an aqueous solution of coenzyme A, lithium carbonate and dithiothreitol (Glover *et al.*, 1991). The desired product was isolated in 45% yield.

2.3. Chemical synthesis

2.3.1. Step *a*. Dodecanolactone. An ice-cooled 250 ml round-bottomed flask was charged with CH_2Cl_2 (40 ml) and $(CH_3CO)_2O$ (26 ml), to which was added H_2O_2 [30%(*w*/*v*), 25 ml]. The mixture was stirred for 1 h, maleic anhydride (0.25 mol, 25 g) was added and stirring at 277 K was continued for 1 h. The mixture was warmed to room temperature, cyclododecanone (0.343 mol, 6.25 g) was added and the mixture was heated to reflux for 15 h. After cooling, the precipitated maleic anhydride was removed by filtration. The filtrate was washed with H_2O (3 × 15 ml), with an aqueous solution containing 10%(*w*/*v*) KOH and 10%(*w*/*v*) Na_2SO_3 (2 × 10 ml), again with H_2O (15 ml), dried (Na_2SO_4), filtered, and concentrated *in vacuo* to give 2-oxacyclotridecanone (dodecanolactone, 7.32 g, 65%) as a yellow oil (Bidd *et al.*, 1983). This crude material was used in the next step without purification.

2.3.2. Step *b*. 12-Hydroxydodecanoic acid. 2-Oxacyclotridecanone (2 g, 10.08 mmol) was heated at reflux (1 h) with KOH (1.5 g) and CH_3OH (10 ml). The mixture was then cooled, concentrated *in vacuo* and partitioned between H_2O (20 ml) and diethyl ether (10 ml). The organic phase was acidified (36% HCl) and the precipitate was isolated by filtration, dried and crystallized from acetone and hexanes to give 12-hydroxydodecanoic acid (1.31 g, 61%) as a white solid, m.p. 358–359 K (357–358 K in Bidd *et al.*, 1983). ^{1}H NMR (DMSO-d_6): 1.16 (br s, CH_2, 14H), 1.45 (m, CH_2, 4H), 2.17 (t, J = 7.2 Hz, CH_2OH, 2H), 3.35 (t, J = 6.5 Hz, CH_2CO$_2$H, 2H), 4.30 (br s, CH$_2$O*H*, 1H), 11.96 (br s, COO*H*, 2H); ^{13}C NMR (DMSO-d_6): 174.73, 60.74, 33.62, 32.52, 29.05, 28.92, 28.51, 25.46, 24.446; IR (KBr): 3249 (OH), 2915, 2849 (CH), 2561 (OH), 1686 (carboxylic acid) cm^{-1}.

2.3.3. Step *c*. 12-Bromododecanoic acid. Acetic anhydride (5 ml) was cautiously added to hydrobromic acid (48%, 2 ml), followed by 12-hydroxydodecanoic acid (1 g, 4.6 mmol). The reaction mixture was heated at reflux for 3 h, cooled and concentrated *in vacuo*. The resulting residue was crystallized from hexanes to give the desired product (0.62 g, 48%) as a white solid, m.p. 328–329 K (327 K in Bidd *et al.*, 1983). ^{1}H NMR (DMSO-d_6): 1.23 (pseudo-s, CH_2, 12H), 1.36 (m, CH_2, 4H), 1.77 (quintet, J = 6.6 Hz, CH_2CH$_2$CO$_2$H, 2H), 2.17 (t, J = 6.9 Hz, CH_2Br, 2H), 3.51 (t, J = 6.9 Hz, CH_2CO$_2$H, 2H), 11.95 (br s, COO*H*, 1H).

2.3.4. Step *d*. 1-Diazo-13-bromotridecan-2-one. 12-Bromododecanoic acid (0.6 g, 2.1 mmol), thionyl chloride (10 ml) and diethyl ether (10 ml) were stirred at room temperature until the evolution of gas ceased. The resulting solution of 12-bromododecanoyl chloride was added dropwise to a 267 K solution of diazomethane in diethyl ether (100 ml) and the mixture was maintained at room temperature overnight. Residual diazomethane was then quenched by the cautious addition of acetic acid and the mixture was concentrated *in vacuo*. The yellow solid was crystallized from hexanes and diethyl ether to give the diazoketone (0.6 g, 97%) as a yellow powder, m.p. 313–312 K. ^{1}H NMR: 1.17 (pseudo-s, CH_2, 14H), 1.55 (m, CH_2CH$_2$Br, 2H), 1.77 (m, CH_2CH$_2$CO,

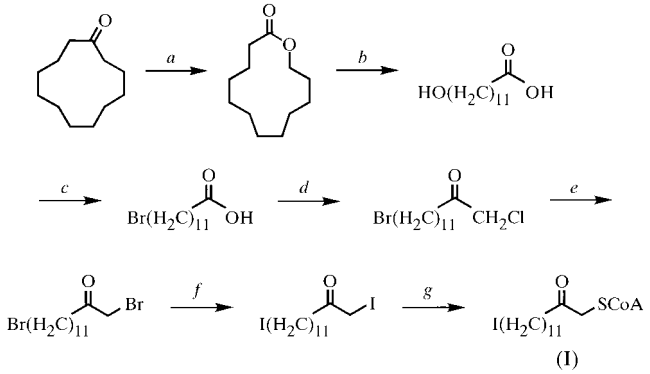

Figure 2
Synthesis of *S*-(13-iodo-2-oxotridecyl)-CoA. Step *a*: Baeyer–Villiger oxidation, H_2O_2, 65%. Step *b*: KOH/CH_3OH; HCl, 61%. Step *c*: HBr/CH_3COOH, 48%. Step *d*: $SOCl_2$, then CH_2N_2, 97%. Step *e*: HBr, 94%. Step *f*: NaI/acetone, 67%. Step *g*: CoASH, 45%.

2H), 2.27 (m, CH_2Br, 2H), 3.35 (m, CH_2CO, 2H), 5.22 (br s, CHN$_2$, 1H); ^{13}C NMR: 195.38, 54.02, 40.82, 33.84, 32.63, 29.23, 29.17, 29.11, 28.98, 28.53, 27.95, 24.98; IR (KBr): 2918, 2851 (CH), 2102 (CH—N$_2$), 1635 (ketone) cm^{-1}.

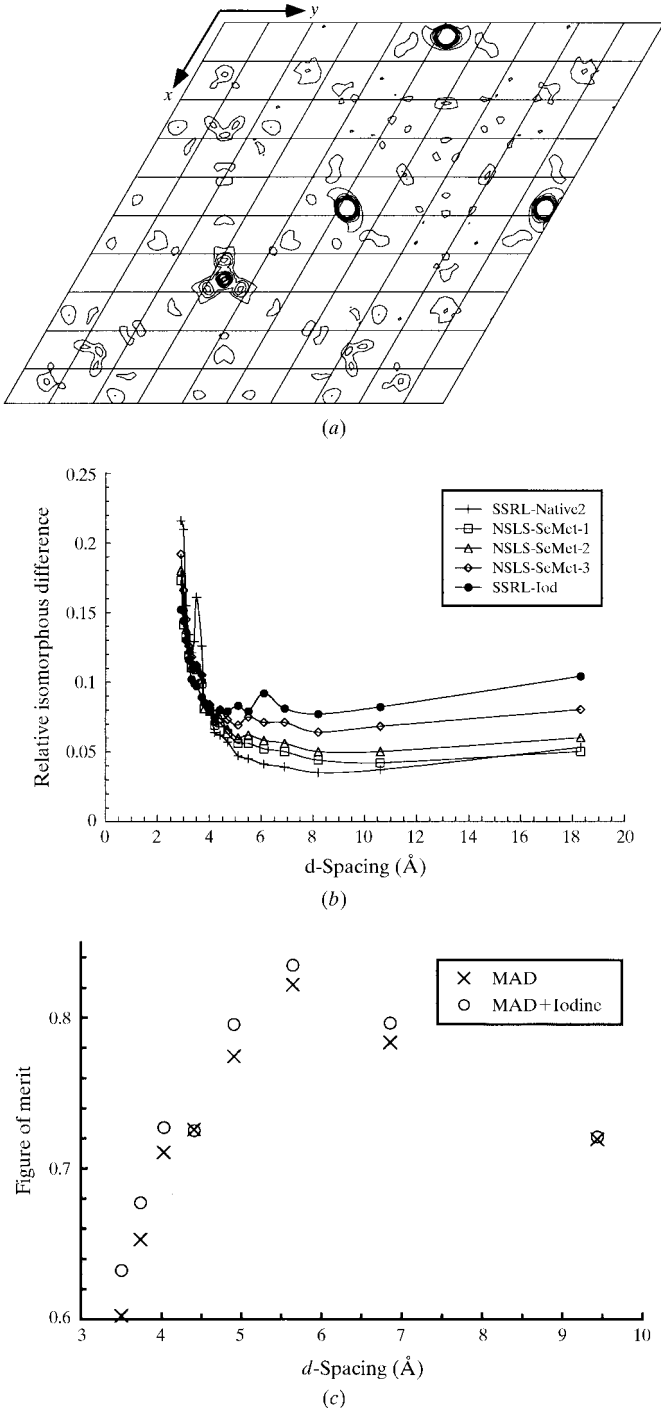

Figure 3
Patterson map, isomorphous difference and figure of merit. (*a*) Harker section (*u*, *v*, 2/3) of the isomorphous difference Patterson map calculated using the SSRL-Native and SSRL-Iod data. (*b*) Relative isomorphous difference as a function of resolution of the data SSRL-Native2, NSLS-SeMet-1 to NSLS-SeMet-3, and SSRL-Iod with respect to SSRL-Native. (*c*) Figure of merit as a function of resolution for MAD phasing and MAD + iodine phasing.

2.3.5. Step e. 1,13-Dibromotridecan-2-one. Hydrobromic acid (0.5 ml, 2.98 mmol) was added to a solution of the diazoketone (0.41 g, 1.4 mmol) in diethyl ether (7 ml) and the mixture was allowed to stir until the effervescence ceased. The mixture was washed with saturated aqueous $NaHCO_3$, dried (Na_2SO_4), filtered and concentrated *in vacuo* to give a crude material that was crystallized from hexanes to give the dibromide (0.47 g, 94%) as a pale yellow solid, m.p. 317–318 K. ^{1}H NMR: 1.23 (pseudo-s, CH_2, 14H), 1.38 (m, CH_2, 2H), 1.57 (m, CH_2CH$_2$Br, 2H), 1.82 (quintet, J = 6.9 Hz, CH_2CH$_2$CO, 2H), 2.61 (t, J = 7.2 Hz, CH_2Br, 2H), 3.36 (t, J = 6.9 Hz, CH_2CO, 2H), 3.86 [s, C(O)CH_2Br, 2H]; ^{13}C NMR (75 MHz; $CDCl_3$): 202.24, 39.63, 34.14, 32.62, 29.21, 29.17, 29.14, 29.06, 28.80, 28.51, 27.94, 23.63; IR(KBr): 2919, 2848 (CH), 1721 (ketone) cm^{-1}.

2.3.6. Step *f*. 1,13-Diiodotridecan-2-one. 1,13-Dibromotridecan-2-one (2.98 g, 8.4 mmol) and NaI (6.93 g, 46.2 mmol) in acetone (25 ml) were stirred at room temperature for 24 h. The mixture was filtered and the filtrate was concentrated *in vacuo*. The residue was then washed with H_2O (50 ml), extracted with CH_2Cl_2 (3 × 50 ml), dried ($MgSO_4$), filtered and concentrated. The product was purified by flash column chromatography [silica gel; ethyl acetate:hexanes 1:20(*v*/*v*)] to give the diiodide (2.54 g, 67%) as a pale yellow solid, m.p. 334–335 K. ^{1}H NMR: 1.35 (m, —CH_2—, 14H), 1.61 (m, CH_2CH$_2$I, 2H), 1.81 (m, CH_2CH$_2$CO, 2H), 2.7 (t, J = 7.5, CH$_2$CH_2I, 2H), 3.18 (t, J = 7.2, 2 H, CH$_2$CH_2CO) and 3.79 [s, C(O)CH_2I, 2H]; ^{13}C NMR: 203.46, 98.61, 39.23, 33.45, 30.36, 29.30, 29.24, 28.86, 28.39, 24.07; IR (KBr): 2847, 2932 (CH), 1712 (ketone) cm^{-1}.

2.3.7. Step *g*. *S*-(13-iodo-2-oxotridecyl)-CoA. Coenzyme A.2H_2O (0.16 g, 0.2 mmol) was dissolved in degassed water (5 ml) at room temperature under N_2. Dithiothreitol (0.004 g, 0.02 mmol) and lithium carbonate (0.06 g, 0.8 mmol) were added. After stirring for 5 min, a freshly prepared solution of 1,13-iodotridecan-2-one (0.2 g, 0.44 mmol) in ethanol (12 ml) was added in one portion. The reaction mixture was stirred at room temperature for 24 h, filtered and the filtrate was concentrated *in vacuo* (water bath <313 K) to give a yellow foam. This material was purified by flash column chromatography [silica gel; *i*-PrOH:MeOH:H_2O (4:3:2)] to give the CoA derivative (45%) as a pale yellow solid, m.p. 433–435 K (dec). ^{1}H NMR (D_2O): 0.54 (s, CH_3, 3H), 0.69 (s, CH_3, 3H), 1.12 (br s, —CH_2—, 16H), 1.33 (m, CH_2, 2H), 1.58 (m, CH_2, 2H), 2.27 [m, NHC(O)CH_2, 2H], 2.44 (m, SCH_2C═O, 2H), 2.65 (m, SCH_2CH$_2$, 2H), 3.27 (m, ICH_2, CH_2NHC═O, CHOH, 7H), 3.65 (m, *H*COP, 1H), 3.83 (m, *H*COP, 1H), 4.05 (m, 5′H, 2H), 4.40 (m, 4′H, 1H), 5.98 (m, 1′H, 1H), 8.06 (m, C-8H, 1H) and 8.37 (m, C-2H, 1H) (45%; note that this compound was used directly to generate the ternary Nmt1p complex).

2.4. Determination of heavy-atom positions

Diffraction data were recorded at beamlines 7-1 of the Stanford Synchrotron Radiation Laboratory (SSRL) and X4A of the National Synchrotron Light Source (NSLS) (see Table 1). Data sets to 2.9 Å resolution were recorded for the ternary complex of Nmt1p bound to *S*-(2-oxopentadecyl)-

Table 1
Data-collection statistics.

Values for the highest resolution shell (2.9–3.0 Å) are given in parentheses.

Data set	Wavelength (Å), beamline	Resolution (Å)	Total/unique reflections	Completeness† (%)	R_{sym}‡ (%)	R_{iso}§ (%)
SSRL-Native	1.08, BL7-1	30–2.9	107670/13909	89.3 (92.9)	7.1 (19.4)	
SSRL-Native2	1.08, BL7-1	30–2.9	79655/14403	91.9 (84.2)	6.9 (27.0)	9.2
NSLS-SeMet-1	0.9792, X4A	30–2.9	98161/14314	91.9 (86.8)	4.4 (20.0)	8.9
NSLS-SeMet-2	0.9789, X4A	30–2.9	96459/14332	92.1 (86.8)	4.6 (21.2)	9.4
NSLS-SeMet-3	0.9668, X4A	30–2.9	94618/14259	91.6 (85.3)	4.9 (23.6)	10.1
SSRL-Iod	1.08, BL7-1	30–2.9	83338/14578	93.4 (87.8)	4.7 (13.8)	9.6

† Completeness for $I/\sigma(I) > 1.0$. ‡ $R_{sym} = \sum|I - \langle I\rangle|/\sum I$, where I is the observed intensity and $\langle I\rangle$ is the average intensity from multiple observations of symmetry-related reflections. § $R_{iso} = \sum ||F_{PH}| - |F_P||/\sum|F_P|$, where F_P is the SSRL-native structure-factor amplitude and F_{PH} is the derivative structure-factor amplitude.

CoA and the dipeptide inhibitor SC-58272 (designated SSRL-Native and SSRL-Native2 in Table 1), for the corresponding selenium-substituted complex (three-wavelength MAD data set designated NSLS-SeMet-1 through NSLS-SeMet-3 in Table 1) and for the ternary complex of Nmt1p bound to *S*-(13-iodo-2-oxotridecyl)-CoA and SC-58272 (designated SSRL-Iod in Table 1).

Nmt1p contains four methionines. The four expected selenium positions were originally determined from isomorphous difference Patterson analysis calculated using the data SSRL-Native and NSLS-SeMet-1 (using the program *HASSP*; Terwilliger & Eisenberg, 1983) and were confirmed by anomalous difference Patterson analysis. Moreover, difference Fourier synthesis on the basis of any three Se-atom positions consistently reproduced the omitted fourth position for all four sites.

An isomorphous difference Patterson map (30–3 Å) using the data SSRL-Native and SSRL-Iod displayed a 20σ peak in the Harker section (u, v, 2/3) (Fig. 3*a*) from which the iodine position was determined using the program *HASSP* (Terwilliger & Eisenberg, 1983). The position was confirmed by isomorphous cross-difference Fourier synthesis using the Se-Met MAD phases and the difference amplitudes between the SSRL-Native and SSRL-Iod data sets. Likewise, phases determined based on the iodine site were sufficient to locate the four selenium sites as major peaks in a cross-difference Fourier synthesis using the anomalous differences of the NSLS-SeMet-1 data set.

2.5. Phasing

The refinement of heavy-atom positions and the phase calculation were carried out using the program *SHARP* (de La Fortelle & Bricogne, 1997), closely following the procedures recommended by the program's authors. The observed structure-factor amplitudes (F_{obs}) were put on a quasi-absolute scale and full occupancy of the selenium and iodine sites was assumed. The anomalous differences of the SSRL-Iod data were included in the refinement of the heavy-atom parameters. Adjustable parameters were floated in a hierarchical fashion, starting with the scale factors, the parameters modeling the isomorphous or, in the MAD case, dispersive differences, then releasing the heavy-atom coordinates and finally the temperature factors. The anomalous contributions to the atomic scattering factor, f' and f'', of Se and I were refined during a separate run keeping all but the scale factors constant. Subsequently, the resulting fitted values of f' and f'' were inserted into a third run of the *SHARP* program. Phases were calculated in the resolution range 30–3.5 Å and were subsequently extended to 2.9 Å during density modification by solvent flipping (program *SOLOMON*; Abrahams & Leslie, 1996).

3. Results and discussion

3.1. Crystallization

The crystallization conditions for the ternary complexes containing *S*-(2-oxopentadecyl)-CoA or *S*-(13-iodo-2-oxotridecyl)-CoA were identical within the bandwidth of reagent concentrations producing crystals [8.5–12%(*w*/*v*) polyethylene glycol 4000, 100 m*M* cacodylate pH 6.25, 50 m*M* zinc acetate, 21.5% glycerol in the reservoir solution; 18% glycerol in the protein solution]. Thus, chemical modification of the ligand did not noticeably affect the crystallization conditions.

3.2. Lack of isomorphism

Incorporation of the iodinated myristoyl-CoA analog did not cause a marked increase in the lack of isomorphism relative to the native ternary complex. Space group and unit-cell parameters were the same within error ($P3_121$; $a = b = 105.4$, c = 106.7 Å). Measuring the relative isomorphous difference (R_{iso}) with respect to the SSRL-Native data (Fig. 3*b*; program *SCALEIT*; Collaborative Computational Project, Number 4, 1994), the SSRL-Iod data display an overall R_{iso} (9.4%, resolution range 30–2.9 Å) that is very similar to the R_{iso} observed between the SSRL-Native and SSRL-Native2 data (9.2%) or between the SSRL-Native and the NSLS-SeMet-1, NSLS-SeMet-2 or NSLS-SeMet-3 data (8.5, 9.4 and 10.1%, respectively). Plotting the isomorphous difference as a function of resolution (d spacing in Å; Fig. 3*b*) reveals that in the low-resolution range (30–4 Å) the SSRL-Iod data display a higher isomorphous difference than the other data used in this structure determination, suggesting an increased lack of isomorphism. However, this difference appears not to be significant and might well be accounted for by differing experimental conditions and data quality.

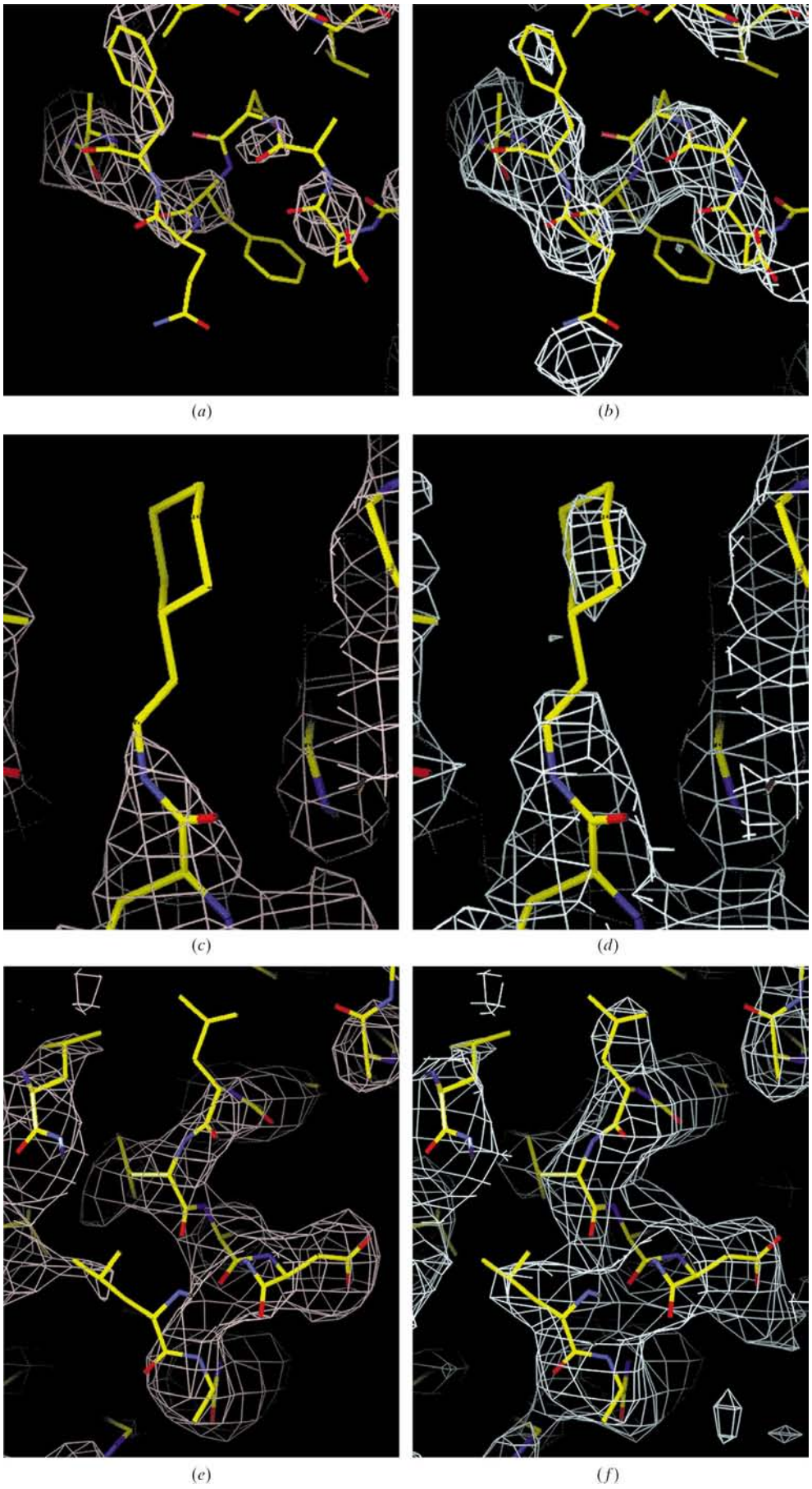

3.3. Electron-density map

A structural model for the ternary complex of Nmt1p bound to *S*-(2-oxopentadecyl)-CoA and SC58272 was initially built based on an electron-density map calculated using the SeMet-MAD phases alone. However, this map contained a number of ambiguous areas, particularly in surface-loop regions, that could not be built with confidence. As a result, only 85% of the backbone structure of the protein could be traced. Adding the SSRL-Iod data to the phase calculation removed those ambiguities and provided a much improved electron-density map overall. In order to assess the contribution of the iodine-derivative data to phasing, we also calculated phases in *SHARP* based on the iodine site alone using the SSRL-Native and SSRL-Iod data sets, including the anomalous differences of the latter. After solvent flattening (using the program *SOLOMON*), the 'iodine-only' map displayed a well defined protein–solvent boundary and was interpretable in most parts (data not shown). However, it was of inferior quality compared with the Se-Met MAD map.

Fig. 4 shows regions of representative experimental electron density calculated either based on Se-Met MAD phases alone (panels *a*, *c* and *e*) or based on 'MAD + iodine' phases (panels *b*, *d* and *f*). For instance, helix αH′ (Figs. 4*a* and

Figure 4
Comparison of solvent-flattened experimental electron density calculated using either MAD phases (panels *a*, *c* and *e*) or 'MAD + iodine' phases (panels *b*, *d* and *f*). The regions depicted are (*a*, *b*) helix αH′, (*c*, *d*) the cyclohexane part of the peptidomimetic SC-58272, (*e*, *f*) helix αI. The stick model represents the refined structure of *S. cerevisiae* Nmt1p. The density map is contoured at 1.2σ.

4*b*; see Bhatnagar *et al.*, 1998 and Weston *et al.*, 1998 for explanations of Nmt's secondary-structure nomenclature) was clearly defined only in the 'MAD + iodine' map. Electron density for the cyclohexane group of the peptidomimetic inhibitor SC-58272 was only apparent in the 'MAD + iodine' map while missing in the Se-Met MAD map (Figs. 4*c* and 4*d*). In many instances, the 'MAD + iodine' map helped to unequivocally identify side-chain orientations, as illustrated in Figs. 4(*e*) and 4(*f*). These examples illustrate the important contribution of the iodine derivative to the quality of the experimental electron-density map. The difference in map quality correlates with the figures of merit (FOM) for the 'MAD + iodine' phases (FOM = 0.728, $\mathrm{FOM_{acentric}}$ = 0.741, $\mathrm{FOM_{centric}}$ = 0.644) compared with the MAD phases (FOM = 0.710, $\mathrm{FOM_{acentric}}$ = 0.727, $\mathrm{FOM_{centric}}$ = 0.597). The higher quality of the 'MAD + iodine' phases also becomes apparent when plotting the FOM as a function of resolution (*d* spacing in Å; Fig. 3*c*).

The 'MAD + iodine' map helped to overcome a major roadblock in building and refining the structure. About 85% of the C^{α} backbone and 65% of all side chains could be unequivocally built based on the Se-Met MAD electron-density map, at which point, however, the refinement stalled with R_{free} = 35.1% and R = 27.3%. Incorporation of the iodine-derivative data in phasing removed ambiguities in the electron-density map and provided the basis for a rapid completion of the structure with final residuals of R_{free} = 29.7% and R = 22.6%.

Given the sequence of events during the course of the structure determination, the question whether the iodine derivative would have been sufficient to determine the structure cannot be answered. However, the structure of *C. albicans* apo-Nmt (Weston *et al.*, 1998) was determined using a single xenon derivative with a single heavy-atom site. Xenon and iodine are immediate neighbors in the periodic table and hence one would expect similar phasing power from these two elements. Building the ternary complex structure of Nmt1p into the 'iodine-only' map would have been difficult but is likely to be possible. Nonetheless, addition of the iodine-derivative data to the Se-Met MAD data had a significant and very beneficial effect on the quality of the experimental electron-density map.

3.4. Generalization of the approach

The approach of using iodinated fatty acids to obtain heavy-atom derivatives of protein–fatty acid complexes appears attractive. The success of this strategy in the case of the ternary complex structure of Nmt1p leads us to suggest that it can be used in a more general fashion. When considering this route to a heavy-atom derivative, two main questions have to be taken into account: (i) the feasibility of chemical synthesis and (ii) the potential steric hindrance preventing binding of the iodine-substituted ligand.

3.4.1. Chemical synthesis. The potential utility of a heavy-atom-modified fatty acid equivalent is much broader than the single example presented here. In principle, the synthetic scheme may be adapted to nearly any fatty acid. Thus, fatty acids of the form $\mathrm{HOCO(CH_2)}_n\mathrm{CH_3}$ can be replaced by their iodinated counterparts $\mathrm{HOCO(CH_2)}_n\mathrm{I}$ or $\mathrm{HOCO(CH_2)}_{n-1}\mathrm{I}$. A general approach would be to use the cyclic ketone having the appropriate number of C atoms in the ring (Fig. 2). Oxidation by the Baeyer–Villiger process would afford the lactone (Fig. 2, step *a*). Hydrolysis and replacement of the hydroxyl group by iodide would afford the ω-iodinated fatty acid.

It should also be noted that this methodology can be extended to other halogens. While the preparation of fluoro- or chloro-substituted fatty acids is of marginal utility to crystallographic analysis, both bromine and iodine offer potential advantages. Iodine and bromine have 53 and 35 electrons, respectively, compared with selenium with 34 electrons which is the most common element used as a heavy-atom marker in MAD experiments. Unlike iodine, the X-ray absorption edge of bromine is located in a readily accessible energy range of synchrotron radiation (*K* edge: 13.5 keV, 0.92 Å) and hence bromine is more suitable for MAD experiments than iodine. Synthetic reactions that are applicable to iodine are normally applicable to bromine as well, although the times and temperatures may have to be altered to accommodate their different reactivities.

3.4.2. Steric hindrance. In Nmt1p, the fatty acid chain is inserted into a deep narrow groove (Fig. 5). The surrounding protein firmly stabilizes the fatty acid chain in its position. Thus, after binding, the fatty acid chain appears to be subject to little thermal motion. Hence, any substitution of C atoms by iodine is likely to lead to a well ordered heavy-atom site, a very desirable property of a derivative. The depiction of the fatty acid binding pocket in Fig. 5 as a molecular surface and CPK rendering of *S*-(13-iodo-2-oxotridecyl)-CoA suggests a

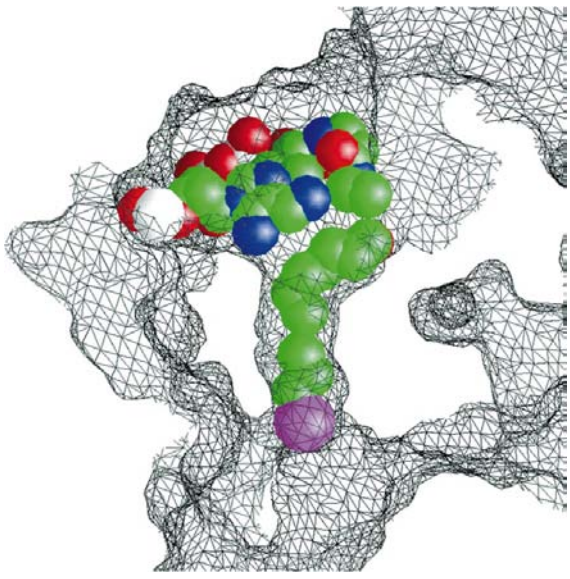

Figure 5
Fatty acyl binding pocket of Nmt1p. The molecular surface of Nmt1p (probe radius 1.4 Å, calculated and displayed in *GRASP*) is shown in grey; *S*-(13-iodo-2-oxotridecyl)-CoA is shown as a CPK model with the I atom in purple.

snug fit of the I atom into the myristate-binding pocket of Nmt1p. The van der Waals (VDW) radius of iodine (2.15 Å) is only a little larger than the VDW radii of either methylene or methyl (2.0 Å). Thus, replacement of either one or two C atoms by iodine in a derivative system could be appropriate.

4. Conclusions

We have shown that the covalent modification of the ω-terminus of the non-hydrolyzable myristoyl-CoA analog *S*-(2-oxopentadecyl)-CoA to *S*-(13-iodo-2-oxotridecyl)-CoA, wherein iodine substitutes the two ω-terminal C atoms, leads to a chemically modified protein–acyl-CoA complex which readily yields crystals under the conditions used for the parent complex. The X-ray diffraction data resulting from the iodinated derivative displayed a moderately increased isomorphous difference relative to the original ternary complex, yet allowed for a straightforward determination of the heavy-atom position. The phasing power of the iodo derivative was weaker than provided by the MAD data, yet sufficient to produce a traceable electron-density map. In combination with the MAD data, the contribution of the iodine derivative was very beneficial and substantially improved the experimental phases.

We suggest that iodination of a fatty acid ligand represents a useful method for obtaining heavy-atom derivatives to determine the structures of protein–fatty acid or acyl-CoA complexes. The only slightly larger van der Waals radius of iodine compared with methyl or methylene would lead us to expect that in most cases the fatty acid binding site can tolerate the carbon-to-iodine substitution, although a significant change in binding affinity caused by the substitution cannot be ruled out. If potential obstacles of chemical synthesis can be overcome, the suggested approach would yield a derivative with two important properties. Firstly, the occupancy of the heavy-atom site would be defined (assuming stoichiometric binding of the ligand). Secondly, it would enable the identification of the ligand-binding site.

This work was supported by grants from the National Institutes of Health (GM-36262 and AI-38200).

References

Abrahams, J. P. & Leslie, A. G. W. (1996). *Acta Cryst.* D**52**, 30–42.
Bhatnagar, R. S., Ashrafi, K., Fütterer, K., Waksman, G. & Gordon, J. I. (2000). *The Enzymes: Protein Lipidation*, 3rd ed., edited by F. Tamanoi & D. S. Sigman, pp. 241–290. New York: Academic Press.
Bhatnagar, R. S., Fütterer, K., Farazi, T., Korolev, S., Murray, C. L., Jackson-Machelski, E., Gokel, G. W., Gordon, J. I. & Waksman, G. (1998). *Nature Struct. Biol.* **5**, 1091–1097.
Bhatanagar, R. S., Fütterer, K., Waksman, G. & Gordon, J. I. (1999). *Biochem. Biophys. Acta*, **1441**, 162–172.
Bhatnagar, R. S. & Gordon, J. I. (1997). *Trends Cell Biol.* **7**, 14–20.
Bhatnagar, R. S., Schall, O. F., Jackson-Machelski, E., Sikorski, J. A., Devadas, B., Gokel, G. W. & Gordon, J. I. (1997). *Biochemistry*, **36**, 6700–6708.
Bidd, I., Kelly, D. J., Ottley, P. N., Paynter, O. I., Simmonds, D. J. & Whiting, M. C. (1983). *J. Chem. Soc. Perkin Trans.*, pp. 1369–1372.
Collaborative Computational Project, Number 4 (1994). *Acta Cryst.* D**50**, 760–763.
Devadas, B., Zupec, M. E., Freeman, S. K., Brown, D. L., Nagarajan, S., Sikorski, J. A., McWherter, C. A., Getman, D. P. & Gordon, J. I. (1995). *J. Med. Chem.* **38**, 1837–1840.
Glover, C. J., Tellez, M. R., Guziec, F. S. & Felsted, R. L. (1991). *Biochem. Pharmacol.* **41**, 1067–1074.
Kishore, N. S., Lu, T., Knoll, L. J., Katoh, A., Rudnick, D. A., Mehta, P., Devades, B., Atwood, J. L., Adams, J. L., Gokel, G. W. & Gordon, J. I. (1991). *J. Biol. Chem.* **266**, 8835–8855.
La Fortelle, E. de & Bricogne, G. (1997). *Methods Enzymol.* **276**, 472–493.
Lu, T., Li, Q., Katoh, A., Hernandez, J., Duffin, K., Jackson-Machelski, E., Knoll, L. J., Gokel, G. W. & Gordon, J. I. (1994). *J. Biol. Chem.* **269**, 5346–5357.
Paige, L. A., Zheng, G.-Q., DeFrees, S. A., Cassady, J. M. & Geahlen, R. L. (1989). *J. Med. Chem.* **32**, 1665–1667.
Rudnick, D. A., McWherter, C. A., Rocque, W. J., Lennon, P. J., Getman, D. P. & Gordon, J. I. (1991). *J. Biol. Chem.* **266**, 9732–9739.
Terwilliger, T. C. & Eisenberg, D. (1983). *Acta Cryst.* A**39**, 813–817.
Weston, S. A., Camble, R., Colls, J., Rosenbrock, G., Taylor, I., Egerton, M., Tucker, A. D., Tunnicliffe, A., Mistry, A., Mancia, F., de La Fortelle, E., Irwin, J., Bricogne, G. & Pauptit, R. A. (1998). *Nature Struct. Biol.* **5**, 213–221.